STRUCTURAL BIOLOGY

Structural insights into phosphatidylethanolamine *N*-methyltransferase PmtA mediating bacterial phosphatidylcholine synthesis

Salma D. Salsabila and Jungwook Kim*

Phosphatidylethanolamine *N*-methyltransferase (PmtA) catalyzes the biosynthesis of phosphatidylcholine (PC) from phosphatidylethanolamine (PE). Although PC is one of the major phospholipids constituting bilayer membranes in eukaryotes, certain bacterial species encode PmtA, a membrane-associated methyltransferase, to produce PC, which is correlated with cellular stress responses, adaptability to environmental changes, and symbiosis or virulence with eukaryotic hosts. Depending on the organism, multiple PmtAs may be required for producing monomethyl- and dimethyl-PE derivatives along with PC, whereas in organisms such as *Rubellimicrobium thermophilum*, a single enzyme is sufficient to direct all three methylation steps. In this study, we present the x-ray crystal structures of PmtA from *R. thermophilum* in complex with dimethyl-PE and *S*-adenosyl-L-homocysteine, as well as in its lipid-free form. Moreover, we demonstrate that the enzyme associates with the cellular membrane via electrostatic interactions facilitated by a group of critical basic residues and can successively methylate PE and its methylated derivatives, culminating in the production of PC.

INTRODUCTION

Phosphatidylcholine (PC) is a pivotal component of lipid bilayers in cells, essential for maintaining membrane integrity and fluidity (*1*, *2*). A deficiency in PC compromises cellular stress responses and the ability to adapt to environmental changes (*3*–*7*). In particular, in correlation of its properties within the membrane (*8*), lack of PC causes antibiotics susceptibilities in *Pseudomonas* (*5*), viability of *Pseudomonas aeruginosa* toward freezing restoration (*6*), and heat-detergent sensitivity in *Agrobacterium tumefaciens* (*7*).

While PC accounts for nearly half of the phospholipids in eukaryotic membranes, its presence in bacterial membranes is highly variable, ranging from 4 to 73% across different species (*9*, *10*). Notably, only about 15% of bacterial species can synthesize PC, predominantly within α-proteobacteria and, to a lesser extent, in β-proteobacteria and Gram-positive bacteria (*10*). For those bacteria that reside in association with eukaryotes, PC deficiency disrupts host-bacteria interactions, impairing symbiosis or virulence with eukaryotic hosts (*7*, *11*–*14*).

There are two major pathways for the biosynthesis of PC in bacteria (Fig. 1). The first pathway involves integral membrane PC synthase, where PC is synthesized through the condensation of cytidine diphosphate diacylglycerol with environmentally acquired choline in a manganese-dependent manner (*15*). The second route, often referred to as the *N*-methylation or de novo pathway, is also conserved in eukaryotes (*16*). This pathway requires three sequential *N*-methylation steps, beginning with phosphatidylethanolamine (PE), progressing to monomethyl-PE (MMPE) and then to dimethyl-PE (DMPE), and ultimately yielding PC. Despite the conservation of *N*-methylation activity across species, substantial variability is observed in the number of PE *N*-methyltransferases (Pmt/PmtA/PEMT) involved, as well as in their amino acid sequences. For instance, mammals have two PEMT isoforms (PEMT1 and PEMT2) (*17*), whereas yeast encode two Pmts (CHO2 and OPI3) with distinct substrate specificity (*18*, *19*). In contrast, most bacteria use a single PmtA to complete all methylation steps (*11*, *20*). The cellular localization of PmtA/PEMT is also species dependent. Bacterial PmtAs are predominantly cytosolic, associating with the cytoplasmic membrane leaflet via electrostatic interactions (*21*, *22*), while eukaryotic PEMTs are integral membrane proteins, located within the mitochondria and endoplasmic reticulum (ER) (*23*).

Bacterial PmtAs are categorized into two distinct families: the *Sinorhizobium* type (S-type PmtA) and the *Rhodobacter* type (R-type PmtA), both of which have diverged within the same superfamily of *S*-adenosyl-L-methionine (SAM)–dependent methyltransferases (*24*). To date, the S-type PmtA from *A. tumefaciens* has been the most extensively characterized, with the ability to catalyze all three transmethylation steps to PC, existing as a monomer that interacts with negatively charged phospholipids to induce membrane curvature (*20*, *21*). In addition, Kleetz and colleagues (*25*) have reported the successful purification of an R-type PmtA from the moderately thermophilic α-proteobacterium *Rubellimicrobium thermophilum*, which encodes a stable, monomeric PmtA capable of catalyzing the complete methylation process to PC. Model structures from AlphaFold suggest that S- and R-type PmtAs exhibit homologous conformations, attributed to the shared Rossmann fold that binds to SAM. However, experimental determination of the three-dimensional (3D) structures of any PmtA variants remains a challenge, likely due to their association with the cytoplasmic membrane leaflet (*22*).

In the present study, we report the first x-ray crystal structure of PE *N*-methyltransferase from *R. thermophilum* (Rt-PmtA) to a resolution of 1.47 Å through single anomalous diffraction method. Our structural analysis revealed two distinct catalytic states of the enzyme: one in complex with *S*-adenosyl-L-homocysteine (SAH) and $DMPE^{18:1/18:1}$ and another with SAH and *n*-dodecyl-β-D-maltoside (DDM), a detergent used to improve the solubility of the recombinant protein. Integrating these structural data with subsequent biochemical investigations, we explored the enzyme's methylation preference, catalytic mechanism, and membrane-binding properties. These combined findings offer comprehensive mechanistic insights into the function of SAM-dependent Pmt/PmtA/PEMT

Department of Chemistry, Gwangju Institute of Science and Technology, Gwangju 61005, Republic of Korea.
*Corresponding author. Email: jwkim@gist.ac.kr

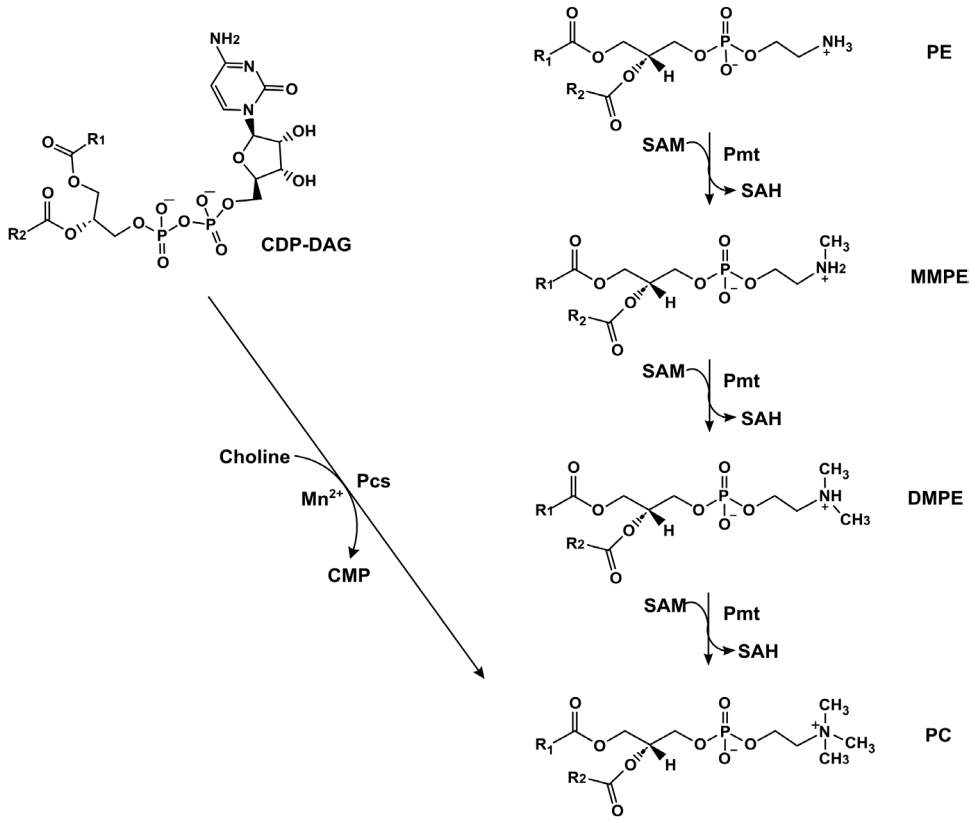

Fig. 1. The two major PC biosynthetic pathways in bacteria. The first pathway involves PC synthase (Pcs), which assembles PC from cytidine diphosphate diacylglycerol (CDP-DAG) and environmentally acquired choline. The second route, referred to as *N*-methylation or de novo pathway, requires three sequential *N*-methylation steps from PE to MMPE, to DMPE, and lastly to PC, using a single or multiple PE *N*-methyltransferases (Pmts).

enzymes in mediating the conversion of PE to PC on the cellular membrane.

RESULTS

MMPE and DMPE are intermediates of *Rt-PmtA* methylations

Despite Rt-PmtA's capability to catalyze all three methylations from PE to PC, *R. thermophilum* lacks MMPE, DMPE, or PE (*25*, *26*). Kleetz and colleagues (*25*) demonstrated that when heterologously expressed in *Escherichia coli*, Rt-PmtA synthesized PC almost exclusively, without producing MMPE or DMPE, whereas the enzyme displayed very weak methylation activities in their in vitro experiments. Therefore, we sought to confirm the presence of MMPE and DMPE as intermediates in the in vitro Rt-PmtA methyltransferase reaction. To this end, we conducted a quantitative methyltransferase assay on $PE^{18:1/18:1}$ using liquid chromatography–tandem mass spectrometry (LC-MS/MS) in multiple reaction monitoring (MRM) mode, where the mass-to-charge ratio (*m/z*) for each lipid species, as well as their fragmentation patterns, was distinctly resolved in the MS/MS analysis. Specifically, the *m/z* values were recorded at 786.6087 for $PC^{18:1/18:1}$, 758.5672 for $MMPE^{18:1/18:1}$, and 772.5838 for $DMPE^{18:1/18:1}$ (Fig. 2 and fig. S1). This analytical technique enabled us to distinguish precisely between the intermediates $MMPE^{18:1/18:1}$ and $DMPE^{18:1/18:1}$ and the final product $PC^{18:1/18:1}$, offering a more accurate detection method than the thin-layer chromatography used in previous studies. Our assay conditions unequivocally resulted in the production of $PC^{18:1/18:1}$, $DMPE^{18:1/18:1}$, and $MMPE^{18:1/18:1}$, where approximately 70% of $PE^{18:1/18:1}$ was transformed into $PC^{18:1/18:1}$ within 1 hour, with only trace amounts of $MMPE^{18:1/18:1}$ and $DMPE^{18:1/18:1}$ observed (Fig. 2). No substantial accumulation of hypomethylated species was detected at any time point, suggesting that $PE^{18:1/18:1}$ is fully methylated by the enzyme in a sequential manner without intermediate release. Therefore, our in vitro assay data strongly support that Rt-PmtA alone is sufficient for efficient synthesis of PC from PE without producing MMPE or DMPE, consistent with the previously reported in vivo results (*25*, *26*).

Rt-PmtA crystallization aided by in situ DDM capturing

To investigate the reaction mechanism of Rt-PmtA through 3D structural analysis, we attempted cocrystallization with various ligands. Initial efforts to crystallize Rt-PmtA in DDM, a detergent used to enhance the solubility of recombinant protein, did not yield crystals of diffracting quality. Subsequently, informed by evidence that excessive detergent can disrupt nucleation and crystal growth by creating free micelles and unstable protein-detergent complexes (*27*), we adopted an "in situ DDM capturing" strategy. This approach has been successfully applied to the crystallization of several membrane proteins, such as the reaction center from *Blastochloris viridis* (*27*), the integral membrane glycerol 3-phosphate acyltransferase from *Aquifex aeolicus* VF5 (*28*), a β-barrel membrane protein from *E. coli* (*29*), and an α-helical aquaporin from spinach leaf plasma membrane (*29*). By using β-cyclodextrin to extract excess DDM, we were able to reduce its concentration from the typical range of 3.86 to 4.8% in

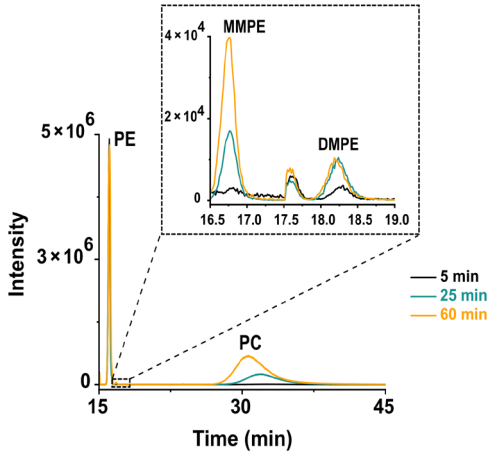

Fig. 2. LC-MS–based quantification of various lipid species from PmtA-directed in vitro assays. The fragment peaks of each lipid species, extracted from MRM LC-MS/MS spectra, were recorded in three different time points after the initiation of each assay and quantified to estimate their relative abundance.

Rt-PmtA samples to 1.3 to 2.5%. This reduction proved crucial for crystallization, leading to the formation of trigonal prism–shaped crystals within 5 days (fig. S2).

Overall structure and topology of Rt-PmtA

Cocrystallization of Rt-PmtA with DMPE$^{18:1/18:1}$ and SAH successfully yielded well-diffracting crystals, as previously mentioned. The x-ray crystal structure of Rt-PmtA was determined to a resolution of 1.47 Å using single-wavelength anomalous dispersion phasing, with crystallographic statistics detailed in Table 1. The asymmetric unit comprises two protein molecules (Fig. 3A): One is complexed with both ligands, while the other binds to SAH and DDM. The two protomers exhibit no substantial protein-protein interface within the x-ray crystal structure, corroborating the previously reported notion that PmtA exists as a monomer biologically (*20*). To substantiate the oligomeric state of the enzyme in solution, we conducted size exclusion chromatography (SEC) on the recombinant protein, where the results are consistent with the monomeric state of Rt-PmtA, as anticipated (fig. S3).

The overall topologies of the lipid-free and lipid-bound protomers are virtually identical, with each primarily composed of a seven-stranded β sheet core flanked by 10 α helices (fig. S4, A and B)—features characteristic of the typical fold found in class I SAM-dependent methyltransferases (*30*). The protomers are superimposable, as evidenced by a root mean square deviation (RMSD) of 0.422 Å (Fig. 3B). A notable difference between the structures is ascribed to the repositioning of His^{117} upon lipid binding, which perturbs key hydrogen bonds that involve His^{117} and Ser^{120} (Fig. 3, C and D). In the lipid-free structure, the side chain of His^{117} on a short helix (α_6) occupies the space that would accommodate the phosphoethanolamine head group, thereby obstructing lipid's access to the active site from the membrane side (fig. S4C). The α_6 becomes a loop in the lipid-bound structure allowing His^{117} to interact with the phosphate group of DMPE. Minor discrepancies are noted in the loop regions between α_3-β_1, β_5-α_8, and β_6-β_7. Meanwhile, DDM's binding mode is distinct from DMPE's, with the detergent molecule primarily engaging with a hydrophobic surface, except for a weak hydrogen bonding interaction between the disaccharide group of DDM and the carbonyl group of Ala^{23} (fig. S4D). DDM's presence in the structure most likely has resulted from nonspecific interactions with the protein or as a crystallization artifact.

Active site and lipid binding pocket of PmtA

Our high-resolution x-ray crystal structure enables the unambiguous determination of the substrate binding sites (Fig. 4A). The cofactor is found in a negatively charged cavity adjacent to DMPE$^{18:1/18:1}$, which is located within a hydrophobic pocket in the center of the protein molecule (fig. S4C). Structural analysis with CAVER (*31*) identified two molecular tunnels within PmtA that span from the SAH binding pocket on the cytosolic side and the DMPE binding site on the membrane side (fig. S5A). The cytosolic end of the tunnel, which accommodates the adenine group of SAH, is located near three loops: β_2-α_5, β_3-β_4, and β_4-α_7. Conformational rearrangement of these loops may play an important role in the opening and closing of the "gate" of this channel.

The binding mode of SAH is identical in both subunits, where the interactions with PmtA are predominantly contributed by loops between β_1-α_4, β_3-β_4, and β_2-α_5 (Fig. 4B and fig. S5B). The polar contacts coordinate the orientation of SAH/SAM ligand, where the side chains of Tyr^{17} and Arg^{29} anchor the carboxylic group of SAH through hydrogen bond and salt bridge interactions. The amino group of SAH forms hydrogen bonds with a pair of carbonyl backbones from Gly^{53} and Met^{116}. Additional polar interactions are formed between the ribose hydroxyl groups of SAH and the side chain of Asp^{73}, a highly conserved residue among Rossmann-folded methyltransferases. Last, the adenine ring of SAH is engaged in hydrogen bonding interactions with the amine backbone of Ala^{74} and Ala^{100} and the side chain of Asp^{99}. The functional importance of these residues for SAM/SAH binding has been confirmed by previous studies, which corroborated that mutations of residues in this region decreased and abolished the SAM binding in vitro in PmtA from *A. tumefaciens* (*32*).

The dimethyl-ethanolamine head group is oriented toward the SAH pocket, which is loosely contained in a pocket lined with mostly hydrophobic residues such as Trp^{13}, Phe^{21}, Val^{121}, and Trp^{172} (Fig. 4, A and C). This structural characteristic may be critical to accommodate the three ethanolamine derivatives of varying sizes. In contrast, the phosphate group of the lipid is contacted by the side chains of Ser^{120} and His^{117}, as well as the backbone amide of His^{147}. These interactions may ensure close contact of ethanolamine head group with SAM. The aforementioned residues are critical for catalysis, as confirmed by our in vitro assays, where mutations resulted in a greater than 90% decrease in enzymatic activity (Fig. 4D). Notably, substitution of Tyr^{10} with phenylalanine rendered the mutant protein essentially inactive, underscoring the critical role of the hydroxyl group on the side chain in catalysis (see Discussion). Meanwhile, the fatty acyl chains of DMPE$^{18:1/18:1}$ are nestled among predominantly hydrophobic residues (Fig. 4C and fig. S5C). Specifically, the *sn*-1 acyl group forms hydrogen bonds with the indole ring of Trp^{172}, while Arg^{156}, Leu^{159}, Met^{163}, and Leu^{200} interact with the fatty acyl chain. The *sn*-2 acyl chain is situated on a hydrophobic surface formed by Ile^{16}, Thr^{20}, Phe^{21}, Val^{24}, Pro^{197}, Leu^{198}, and Met^{201}.

Membrane association mechanism of Rt-PmtA is primarily driven by ionic interactions

It has been proposed that the N-terminal helical motif of PmtA plays a dual role in both catalysis and membrane association, as suggested

Table 1. Data collection, processing, and structure refinement statistics. Values in parentheses correspond to highest-resolution shell.

	Rt-PmtA-DDM-DMPE-SAH
Data collection	
Space group	$P2_12_12_1$
Cell dimensions	
a, *b*, *c* (Å)	71.04, 77.68, 83.16
α, β, γ (°)	90, 90, 90
Wavelength (Å)	0.97957
Resolution (Å)	56.77–1.46 (1.49–1.46)
R_{merge}	0.105 (4.307)
R_{meas}	0.109 (4.477)
R_{pim}	0.029 (1.215)
Total reflections	1,076,009 (52,998)
Unique reflections	79,982 (3943)
$I/\sigma(I)$	13.2 (0.7)
Completeness (%)	100.0 (100.0)
Multiplicity	13.5 (13.4)
$CC_{1/2}$	1.000 (0.322)
Wilson B-factor (Å^2)	20.8
Refinement	
Resolution (Å)	56.77–1.46
Reflections used in refinement	79,830
Reflection used for free set	3983
R_{work}/R_{free}	0.152/0.197
Protein residues	416
No. of protein in asymmetric unit	2
No. of atoms	
Protein	3,239
Ligand/detergent/ion	160
Water	336
Average B-factors (Å^2)	
Protein	25.33
Ligand/detergent/ion	26.99
Water	34.73
RMSDs	
Bond lengths (Å)	0.011
Bond angles (°)	1.782
Ramachandran favored (%)	98.0
Ramachandran allowed (%)	2.0
Ramachandran outliers (%)	0.0
Protein Data Bank code	8YS9

by structural modeling and liposome cosedimentation assays (*21*, *22*). In an attempt to unveil the precise region on the protein involved in membrane engagement, we first identified potential membrane-interacting residues using our x-ray crystal structure as an input to PPM 3.0 Web server (*33*). The generated model proposes that the amphiphilic α helices (α_2, α_8, and α_9) and β_6-β_7 loop are pivotal in mediating membrane association (Fig. 5A). Notably, conserved arginine residues within these helices and the loop are positioned to potentially engage with a planar membrane structure through electrostatic interactions. We selected a total of seven arginine residues situated less than 8 Å away from the membrane curvature for targeted mutagenesis studies. These residues aggregate into roughly three distinct groups on the protein surface: Group 1 comprises Arg^{12} and Arg^{19} on α_2; group 2 consists of Arg^{153}, Arg^{156}, Arg^{161}, and Arg^{169} spanning α_8-α_9; and group 3 is represented by Arg^{199} on the β_6-β_7 loop (Fig. 5, A and B). To investigate their role in membrane association, we engineered three mutant proteins by substituting arginine residues with glutamates in each group, designated M1, M2, and M3.

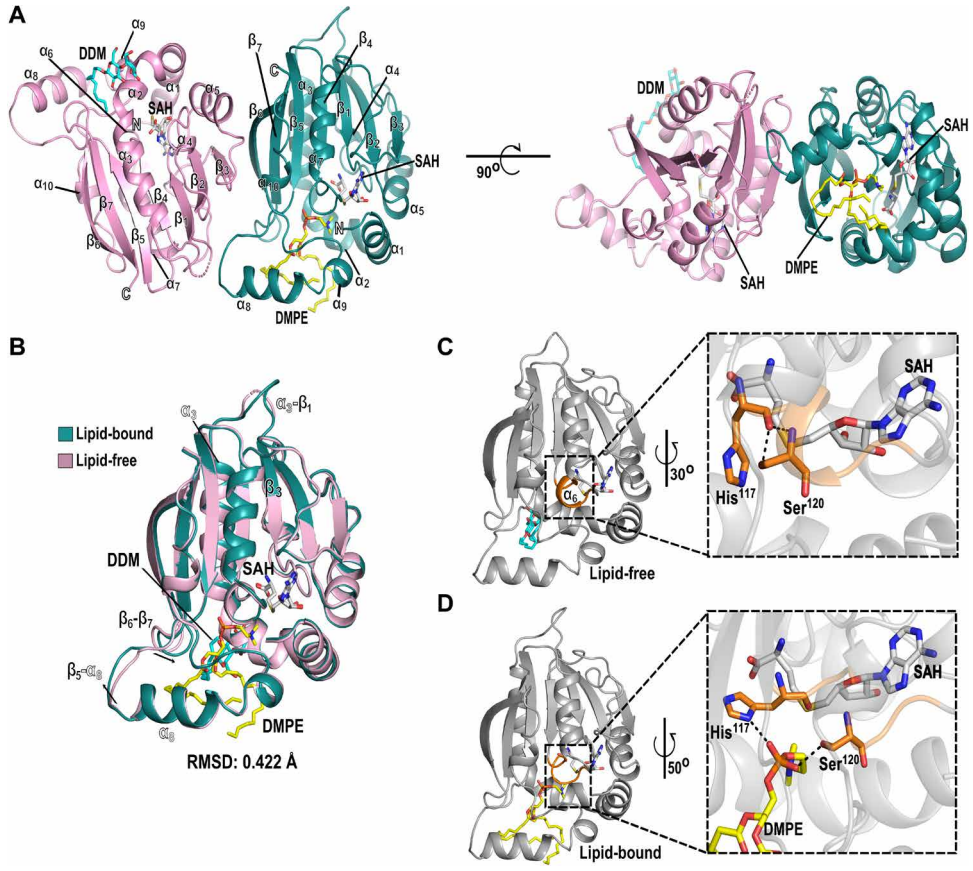

Fig. 3. Overall structure of Rt-PmtA. (**A**) The asymmetric unit contains two Rt-PmtA protomers: one (in deep teal) complexed with DMPE (yellow) and SAH (gray), termed "lipid-bound," and the other (in light pink) with DDM (light blue) and SAH, termed "lipid-free." (**B**) The structural alignment of lipid-free (pink) and lipid-bound (deep teal) forms. RMSD, root mean square deviation of the α-carbons. (**C** and **D**) A local conformational change in each state is highlighted in insets. The presence of a short helix, α_6 (orange), is shown in the lipid-free structure (C) but absent in the lipid-bound form (D). This conformational transition of appears to be driven by the reorientation of His^{117} upon lipid binding, disrupting hydrogen bonding interactions with Ser^{120}.

The membrane association of recombinant Rt-PmtA expressed in *E. coli* was then quantified by analyzing the protein's distribution between bacterial membrane and cytosolic fractions using Western blot, using a NaCl gradient in the lysate buffer that ranged from 150 to 500 mM. As hypothesized, wild-type PmtA exhibited a gradually decreased affinity for the membrane with increasing NaCl concentration, with PmtA membrane–bound fraction reduced from 70 to 30% (Fig. 5, C and D). This pattern is consistently observed with the mutant proteins, where their membrane affinity is notably weaker compared to the wild type. For instance, the M2 variant with quadruple R-to-E substitutions displays negligible membrane association even under isotonic conditions, supporting the notion that PmtA uses these C-terminal helices to bind with the negatively charged lipids on the inner membrane.

DISCUSSION

The distinct structural features of methyltransferase PmtA

We report a high-resolution x-ray crystal structure of ligand-bound Rt-PmtA, a SAM-dependent methyltransferase acting on PE, MMPE, and DMPE to yield PC on the bacterial membrane. Besides the common Rossmann-fold conserved among numerous methyltransferases, our structure features a unique conformation compared to other members. The top five structural homologs of Rt-PmtA identified by the DALI server (*34*) are 24-sterol C-methyltransferase, UbiE/COQ5 methyltransferase, magnesium-protoporphyrin *O*-methyltransferase, nodulation protein S, and an uncharacterized methyltransferase YcgJ, all with RMSD of approximately 2.5 Å (fig. S6A). The superposition of Rt-PmtA with these structural homologs illustrates the shared methyltransferase core but highlights the largest conformational divergence in the C-terminal region (corresponding to Rt-PmtA's α_8 and α_9) (fig. S6B), which is responsible for membrane association and lipid binding as demonstrated by our structure-guided membrane association experiments (Fig. 5). The low sequence identity and functional diversities of these structural neighbors further highlight the unique structural feature of Rt-PmtA, a peripheral membrane protein, which is able to add methyl groups to the PE derivatives on the bacterial membrane.

Structural comparison between R-type and S-type PmtA

Despite the R-type and S-type PmtA carrying out a similar biological function, they share less than 20% sequence identity. It is challenging to compare structures of PmtA from each type since no other structure is available besides ours. We performed pairwise structural comparisons of Rt-PmtA structure with AlphaFold (*35*) of various PmtAs from other species, including *Thermobifida fusca*,

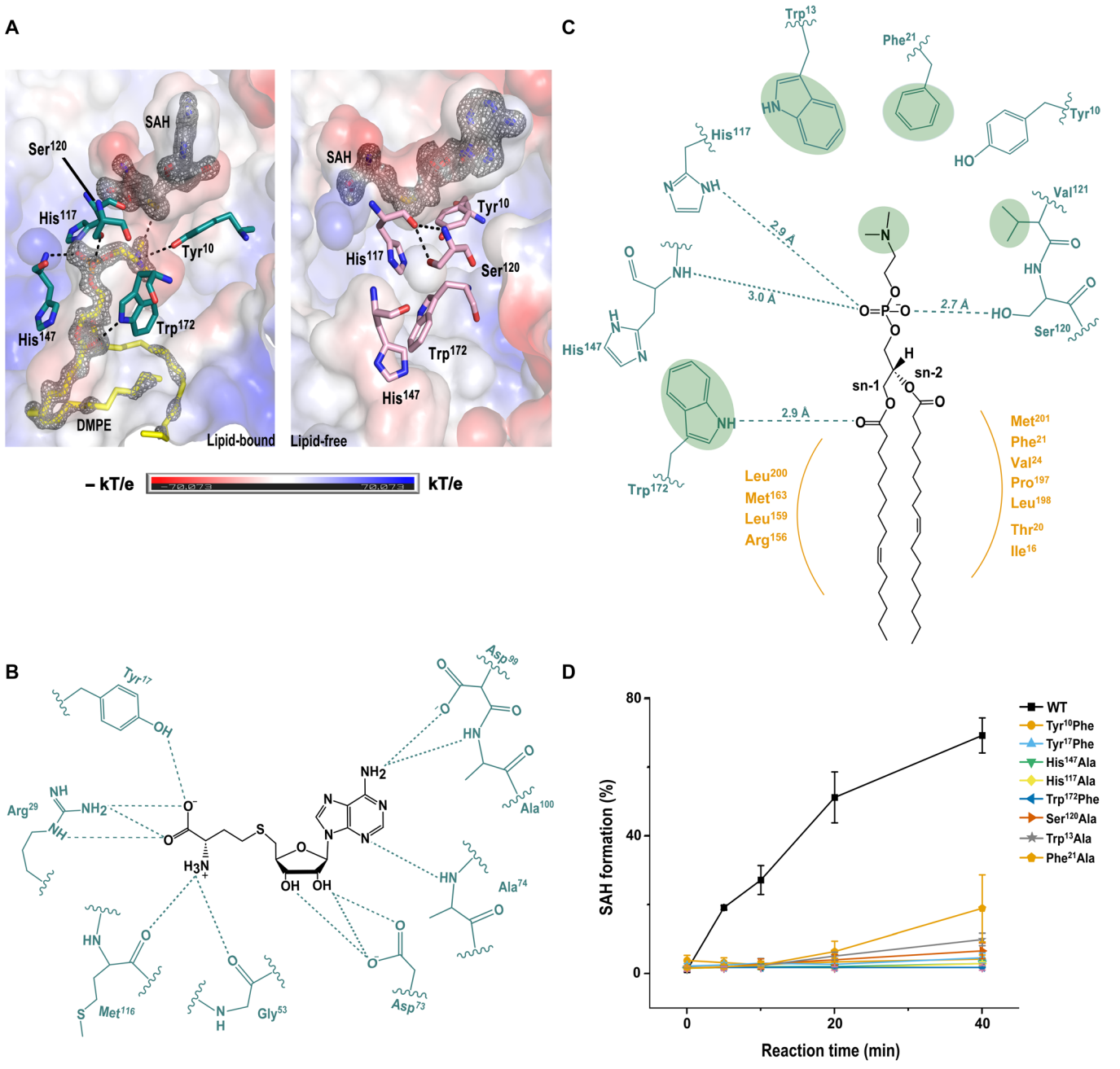

Fig. 4. Structural basis for the ligand recognition. (**A**) The comparison of the active sites of lipid-bound and lipid-free structures with Fourier difference maps (Fo-Fc) for DMPE$^{18:1/18:1}$ and SAH in gray mesh at 3σ contour. Amino acids displaying a notable conformational change are labeled and shown in sticks. (**B**) SAH's polar interactions with Rt-PmtA residues are depicted in dotted lines. (**C**) Intermolecular interactions between DMPE$^{18:1/18:1}$ and active site residues. Hydrogen bonds are shown in deep teal dashed lines, whereas key amino acid residues forming hydrophobic interactions with the ethanolamine group of the bound lipid are displayed in green circles. The residues labeled in orange denote those that interact with the acyl chains of the lipid substrate. (**D**) In vitro assays of the wild-type (WT) and mutant Rt-PmtA, where the time course of SAH formation was recorded. The error bars represent the SD from three independent measurements at each time point.

Thermostaphylospora chromogena, *Xanthomonas campestris*, *Melghirimyces thermohalophilus*, *A. tumefaciens*, and *Sinorhizobium meliloti* that belong to S-type PmtA, and *Rhodobacter sphaeroides*, *Legionella pneumophila*, and *Acetobacter aceti* to represent R-type PmtA. For analyses, we used the DALI server to score the quality of structural alignments and to calculate the RMSD values (*34*). When the structures of R-type PmtA were superimposed with that of Rt-PmtA, the *z*-scores ranged from 25.8 to 31.8 with RMSD values between 1.3 and 2.0 Å (fig. S7A). Meanwhile, the models of S-type PmtA aligned much poorer than the R-type, with *z*-scores ranging between 14.0 and 15.8 and RMSD values from 2.7 to 3.0 Å. Apparently, the most notable conformational deviation occurs in the C-terminal helical region, which was shown to be functionally important in our study with Rt-PmtA. The C-terminal helical feature is well conserved in

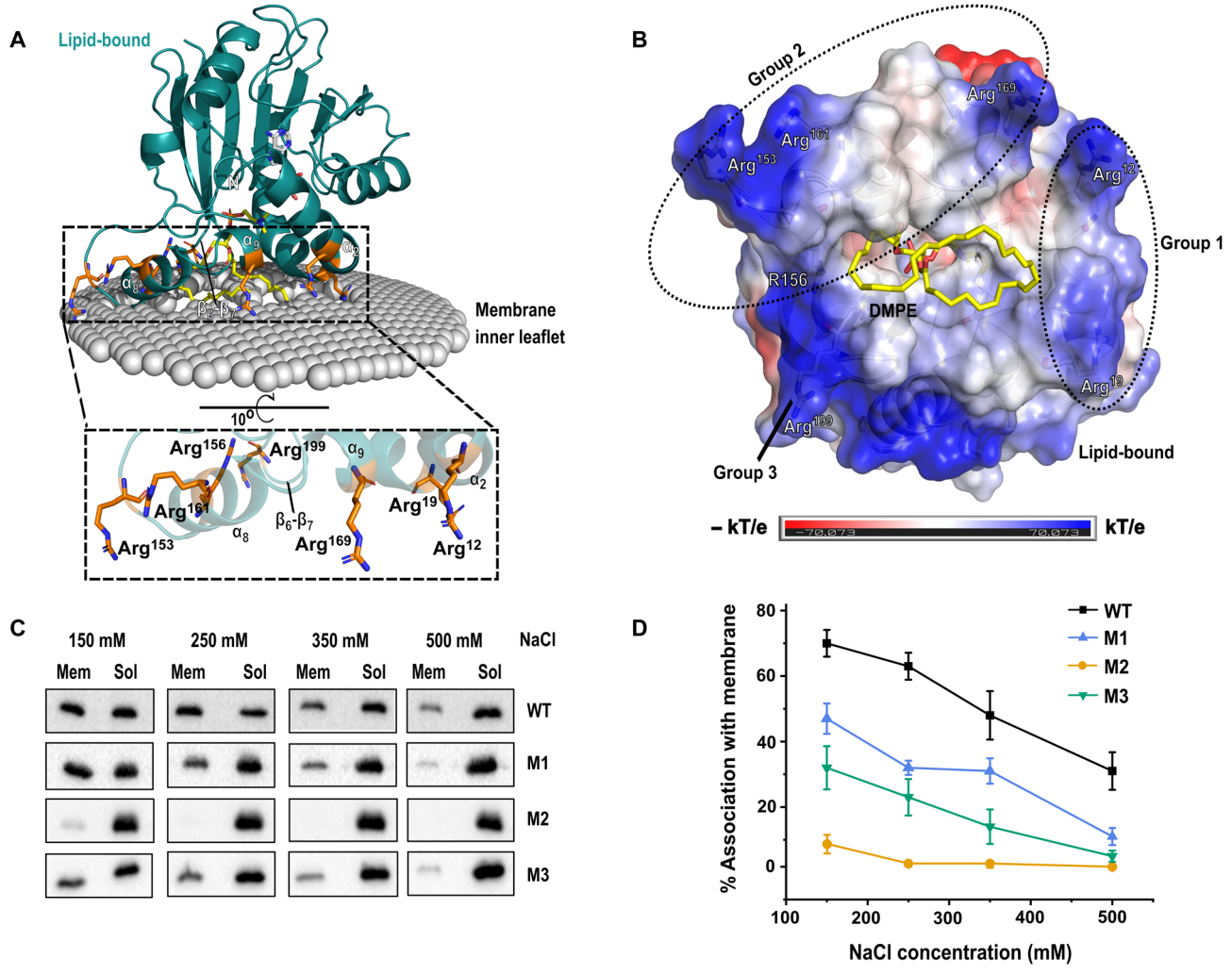

Fig. 5. Membrane association of Rt-PmtA via electrostatic interactions. (**A**) A model of lipid-bound Rt-PmtA interacting with the inner leaflet of the cellular membrane based on PPM server analysis. An inset provides a close-up view of critical basic residues (orange sticks) at the interface, highlighting their potential role in membrane interaction. (**B**) The electrostatic potential (blue, positive; white, neutral; red, negative) and arginine residues involved in membrane association are mapped on the surface model of Rt-PmtA. These basic residues are pooled into three groups for the creation of glutamate mutants (M1, M2, and M3), aiming to assess their membrane affinity as depicted in (C). (**C**) A representative Western blot demonstrating the cellular distribution of wild-type and mutant Rt-PmtA across different NaCl concentrations. (**D**) Quantitative analysis of the Western blot results, where error bars represent SD from three independent experiments.

the R-type homologs as in Rt-PmtA (fig. S7, B and C). Moreover, the R-types exhibit a microenvironment around the putative active sites analogous to Rt-PmtA, i.e., conservation of amino acid residues corresponding to Tyr^{10}, Ser^{120}, and His^{147} (figs. S7C and S8). Structural comparison of active sites with the S-type is not feasible because of a high degree of diversity. Our structural analyses indicate that unique strategies for lipid binding and catalysis are in place among the two distinct evolutionary lineages of bacterial PmtA.

Catalytic mechanism of Rt-PmtA

The pK_a (where K_a is the acid dissociation constant) of ethanolamine and its derivatives is estimated to be around 9.5, indicating that activation of the amine through a deprotonation step is necessary for optimal activity. Our mutagenesis experiments showed that the activity of the Tyr^{10}Phe mutant decreased substantially, implying the catalytic significance of the 4-hydroxyl group on the phenol side chain. Given that this functional group is positioned closest to the nitrogen atom of the ethanolamine moiety, at approximately 3.7-Å distance, it is plausible that the absolutely conserved Tyr^{10} serves as a general base, thereby enhancing the nucleophilicity of the amine (Fig. 6A). In addition, the backbone carbonyl group of Gly^{171} and the phenolic side chain of Tyr^{10} form a hydrogen bond in the structure, which may contribute to lowering the pK_a of Tyr^{10}, thus shifting the equilibrium toward the anionic state. These two residues are also highly conserved among the R-type PmtA (fig. S8).

Moreover, the hydrophobic nature of the active site pocket around the amine group of lipid substrate may promote the stabilization of the unprotonated state, contributing to the activation of the nucleophile. Therefore, once deprotonated, the amine group can retain sufficient nucleophilicity toward SAM for the subsequent methylation steps. Our in vitro assay results showed that the methylation occurs consecutively with PE$^{18:1/18:1}$, which is presumed to be more

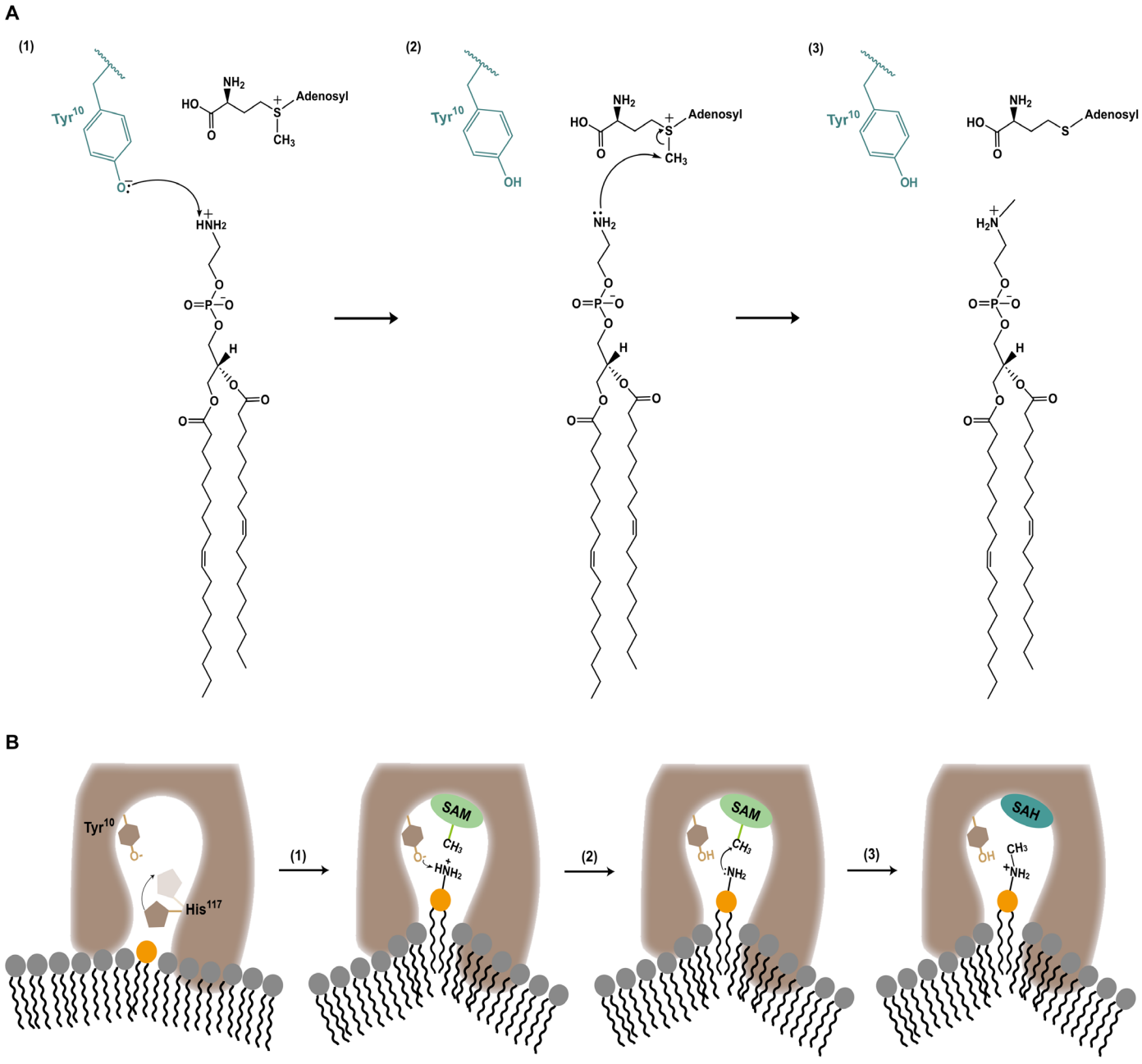

Fig. 6. A proposed reaction mechanism of Rt-PmtA. (**A**) (1) Tyr^{10} acts as a general base in activating the ethanolamine group of PE. (2) The activated amine attacks the *S*-methyl group of SAM to form MMPE (3). (**B**) A unified molecular mechanism of Rt-PmtA on the bacterial membrane. (1) The PmtA-membrane attachment triggers the local membrane curvature for PE to access the active site tunnel. Partial extraction of PE from the membrane is aided by relocation of His^{117}. (2) Tyr^{10} deprotonates from the ethanolamine of PE. (3) The resulting amine nucleophilically attacks the *S*-methyl group of SAM, leading to the formation of MMPE. Two additional repetitions complete the production of PC.

thermodynamically favorable than a model where a hypomethylated intermediate is released from and rebinds to the active site for the next round. We speculate that the hydrophobic interaction between the active site and the neutral amine group of lipid substrate drives the elimination of protons from the amine group, thereby preventing the release of intermediates and enabling subsequent methylation. Conversely, this nonpolar environment in the active site may also facilitate the release of the final product, PC, a quaternary amine that bears a positive charge with no removable proton. The fact that the hydrophobic amino acid residues around the dimethyl-ethanolamine group are highly conserved among R-type homologs (>90%) (fig. S8), with occasional substitutions by other nonpolar residues, reinforces our hypothesis on the critical role played by the unique polarity of the active site in distinct molecular interactions with both the substrate and product.

In summary, we propose the following reaction mechanism (Fig. 6B): Rt-PmtA engages with the membrane predominantly via a

set of key arginine residues. Upon binding to the membrane, PE is partially extracted from the lipid layer, likely accompanied by membrane restructuring to facilitate this process, as observed with other PmtAs (*22*, *36*). The entrance of PE into the active site of Rt-PmtA is regulated by the bulky side chain of His^{117}. Tyr^{10} then activates the nucleophilic amine group of the lipid, acting as a general base to facilitate all three consecutive methyl transfer reactions from SAM, ultimately yielding PC.

MATERIALS AND METHODS

Materials

For purification, crystallization, and enzymatic assay DDM from Carbosynth (San Diego, CA) was used as a detergent to enhance the solubility of the recombinant Rt-PmtA. The β-cyclodextrin for removing excess DDM was obtained from Tokyo Chemical Industry (Tokyo, Japan). SAM used in the assay was from Santa Cruz Biotechnology (Dallas, TX). All lipid substrates were purchased from Avanti Polar Lipids (Alabaster, AL). All commercial reagents were used without further purification.

Cloning and mutagenesis

The *ruthe-01610* gene from *R. thermophilum* DSM 16684 strain (National Center for Biotechnology Information Bacterial Genome Database), which encodes Rt-PmtA, was codon-optimized (*37*) and synthesized by Integrated DNA Technologies. The synthetic gene was amplified by polymerase chain reaction using Phusion Plus DNA Polymerase (catalog no. F630XL, Thermo Fisher Scientific) and inserted into LIC-pLATE31 and LIC-pLATE51 vector (catalog nos. K1261 and K1251, Thermo Fisher Scientific) following the manufacturer's methods to generate recombinant Rt-PmtA fused with the C-terminal and N-terminal His-tag. The site-directed mutagenesis in Rt-PmtA was introduced by adapting in vivo cloning method (*38*). All construct sequences were verified by Macrogen, South Korea. The optimized gene sequence and designated primers used in this study are summarized in table S1.

Protein expression and purification

The Rt-PmtA-pLATE31 was used for crystallization and mutagenesis study, while the Rt-PmtA-pLATE51 was used for enzyme's biological assembly and membrane association assay. *E. coli* BL21(DE3) carried the expression vector was grown in Luria-Bertani medium supplemented with ampicillin (100 mg/ml) at 37°C with rigorous shaking at 160 rpm until optical density at 600 nm (OD_{600}) = 0.4 to 0.8. The expression was induced by adding isopropyl β-D-thiogalactopyranoside (IPTG) to a final concentration of 0.5 mM for the wild type or 1 mM for mutants. Further incubation was conducted at 37°C with rigorous shaking at 160 rpm for 4 to 5 hours. The cells were collected by centrifugation at 14,372 rcf for 15 min at 4°C and resuspended in buffer A [50 mM tris-HCl (pH 8), 500 mM NaCl, 10% (v/v) glycerol, and 50 mM imidazole]. The resuspended cells were supplemented with 2 mM dithiothreitol, 1 mM phenylmethylsulphonyl fluoride, and lysozyme (1 mg/ml) and then incubated at 25°C with rocking for 20 min. The cells were broken by sonication with 50% amplitude. The membrane protein was solubilized by incubating cell lysate at 4°C for 1 hour with DDM to a final concentration of 1% (w/v). The cell debris and insoluble fractions were removed by centrifugation at 21,672 rcf for 30 min at 4°C. After 0.2-μm pore size filtration, the supernatant was applied onto HisTrap HP 5 ml column (Cytiva, USA) equilibrated with buffer A containing 0.1% (w/v) DDM. The His-tagged Rt-PmtA bound to the column was eluted by 50 to 500 mM gradient concentration of imidazole. Further purification was performed by loading eluted samples onto SEC column (Superdex 75 10/300 GL, GE Healthcare) and prechilled with buffer B [30 mM tris-HCl (pH 8), 150 mM NaCl, and 10% (v/v) glycerol] containing 0.05% (w/v) DDM. The overall folding integrity of purified proteins, including the wild type and all mutants, was confirmed by SEC and circular dichroism (CD) analyses (fig. S9). The purified protein was collected, flash-frozen, and stored at −86°C until used.

The selenomethionine (SeMet) substitution was prepared by culturing the *E. coli* BL21(DE3) carrying Rt-PmtA wild type in M9 minimal media containing ampicillin (100 mg/ml) at 37°C with 160 rpm, rigorously shaking until OD_{600} = 0.4 to 0.7. The threonine, lysine and phenylalanine (100 mg/liter) and valine, isoleucine, leucine, and SeMet (50 mg/liter) were added, and additional shaking continued for 15 min before induction by 1 mM IPTG at 37°C (*39*). The cells were harvested after 13 hours and purified following similar method with native protein. Except, all buffers used were degassed and supplemented with tris(2-carboxyethyl)phosphine (Sigma-Aldrich) to a final concentration of 5 mM (in lysis) and 0.2 mM (in purification steps).

β-Cyclodextrin treatment for excess DDM removal

In situ removal of DDM was taken by adapting Li and colleagues (*28*, *40*) method with slight modification. Briefly, the 2-ml concentrated native (2 mg/ml) or SeMet (4 mg/ml) Rt-PmtA was diluted with 10 mM β-cyclodextrin in buffer B at 2.25-fold volume. The diluted sample was concentrated until 1 ml using Amicon Ultra-15 centrifugal filter 50-kDa molecular mass cutoff (Millipore, MA). The 1-ml sample was rediluted at 2.2-fold, reconcentrated until 1 ml, rediluted again at 2-fold, reconcentrated to 1.5 ml, and reexchanged buffer into buffer B two times. Last, the Rt-PmtA samples were reconcentrated to a final concentration of 5 mg/ml for crystallization attempt.

Quantification of DDM concentration

The measurement of DDM concentration was based on quantification of total sugar at an absorbance of 490 nm (*28*, *40*, *41*). A standard curve was prepared using DDM standard solution in the range of concentration of 0.02 to 0.1% (w/v), in which the linear regression was used to determine the correlation between the DDM concentration and absorbance at 490 nm. Following steps were performed under fume hood. The DDM standard solution of 50 μl was pipetted into 700 μl of concentrated sulfuric acid in a 1.5-ml Eppendorf tube. After mixing thoroughly, 140 μl of 5% (w/v) phenol was added and let it stand for 10 min. Because of the exothermic nature of the reaction, the temperature elevated to 110° to 120°C, and the reaction tube was allowed to be cooled down to 25°C in heat block. The tube was vortexed for 30 s, followed by 20 min of incubation for color development. The protein samples were diluted 100-fold before the assay and measured following identical steps.

Quantification of each lipid species in Rt-PmtA methyltransfer reaction via MRM

The reaction condition for the assay adopted from previous study (*25*). The reaction mixture in 200 μl containing 30 mM tris-HCl (pH 8), 150 mM NaCl, 10% (v/v) glycerol, 4 mM SAM, 0.05% DDM, and 1 mM of $PE^{18:1/18:1}$ substrate was briefly sonicated and preincubated at 30°C for 2 min. The reaction was initiated by adding 1 μM

Rt-PmtA to the reaction mixture above, followed by the incubation at 30°C. The reaction was terminated in time-dependent manner (0, 15 min, 30 min, 45 min, and 1 hour of incubation) by lipid extraction method, which was developed by Folch *et al.* (*42*). The extracted lipids in lower phase were dried out by heating on the hot plate and resuspended in 100 μl of 99% (v/v) methanol, which were subjected to analyses by LC-MS.

Ten microliters of each sample was injected to the reversed-phase high-performance LC (HPLC) column [Intensity Solo 2 C18, 2.0 mm, 2.1 mm by 100 mm, BRHSC18022100, B2328 (Bruker, USA)] attached to elute LC series (Bruker, USA). The gradient elution was performed using solvent A [0.1% (v/v) formic acid in acetonitrile:water: 1 M aqueous ammonium formate (600:390:10 (v/v/v)] and solvent B [0.1% (v/v) formic acid in isopropanol:acetonitrile:1 M aqueous ammonium formate (900:90:10 (v/v/v)] under the flow rate of 0.4 ml/min. The first 1-min 50% solvent B was applied, followed by linear gradient from 50 to 99% B for 24 min, and hold for 20 min. With linear gradient, the solvent B decreased from 99 to 50% for 10 s and lastly hold at 50% B for 9.9 min. MS and MS/MS data were acquired on Impact II QTOF MS (Bruker, USA) by full scan ranged 50 to 1000 *m/z* in positive electrospray ionization mode with 500-V endplate offset, 4500-V capillary, 1.2-bar nebulizer, dry gas (10 liter/min), and 200°C dry temperature. For quantification of lipid species, MRM mode was applied to the MS/MS step. Identification of the PE, MMPE, DMPE, and PC peaks was based on the measurement of *m/z* values and fragmentation pattern of respective like compounds with aid of LIPID MAPS structure database and human metabolome database (*43*, *44*). The peaks were extracted from MZmine2 software (*45*) and plotted in Origin 2023 software.

Methylating activity of Rt-PmtA mutants via HPLC

Methylating activity analysis via HPLC was adapted from Yoo *et al.* (*46*). Twenty-five microliters of assay mixture contained 100 μM SAM, 50 μM DMPE$^{18:1/18:1}$, and 1 μM Rt-PmtA (wild type or mutants) in buffer B containing 0.05% DDM. The SAM and DMPE were mixed and sonicated briefly, before adding the Rt-PmtA. The reaction was carried out at 30°C for 0, 5, 10, 20, and 40 min. At each time point, all reactions were quenched by 0.05% (v/v) formic acid. The analysis aimed to quantify SAM and SAH peak by injecting terminated samples onto normal phase HPLC column, specifically the SeQuent ZIC-HILIC Column, 200 Å, 5 μm, 4.6 mm by 150 mm. All parameters and solvent gradient steps were followed according to Yoo *et al.* (*46*).

Crystallization

For crystallization, proteins eluted from HisTrap column were buffer exchanged into buffer B containing 0.05% (w/v) DDM using Amicon Ultra-15 centrifugal filter 10-kDa molecular mass cutoff (Millipore, MA), instead of performing SEC step. It was then further treated by "in situ removal of DDM" method.

The crystallizations were set up using hanging-drop vapor diffusion method in 24-well VDX plates (Hampton Research) at 20°C, where 1.5 μl of protein mixture solution was mixed with an equal volume of mother liquor and the mixture was equilibrated against 400 μl of mother liquor. To obtain native crystals of PmtA-DMPE$^{18:1/18:1}$-SAH, a mixture of 0.2 mM (4.5 mg/ml) Rt-PmtA, 1 mM DMPE$^{18:1/18:1}$, and 0.4 mM SAH was prepared, and an equivalent volume of the crystallization cocktail containing 0.4 M ammonium sulfate, 0.1 M potassium sodium tartrate tetrahydrate, and 20% (v/v) polyethylene glycol 3350 was added. The SeMet-labeled crystals of PmtA-DMPE$^{18:1/18:1}$-SAH were obtained in an essentially identical method. Both crystals were observed within a week, then fished with a CryoLoop (Hampton Research), and directly cryocooled into liquid nitrogen without additional cryoprotectant.

X-ray data collection and structural determination

All x-ray diffraction experiments were performed at beamline 5C of Pohang Accelerator Laboratory (South Korea) equipped with EIGER X 9M detector under cryogenic condition. All datasets were collected at wavelength = 0.9795 Å. Diffraction data were indexed, integrated, and scaled using AutoPROC (*47*). The crystallographic statistics are summarized in Table 1.

The phase problem was solved by experimental phasing through single-wavelength anomalous dispersion with Crank2 that provided in CCP4Cloud Remote v.1.7.002 (*48*–*50*). The model structure was built by sequential iterative real-space model building by Coot (*51*) and refinement by REFMAC5 (*52*). The model was later used as search model for molecular replacement with MOLREP to solve the native Rt-PmtA structure. The 3D model of DMPE$^{18:1/18:1}$ was created using AceDRG and fitted in the ligand-free structure of the enzyme using WinCoot. The structures were visualized by PyMOL (*53*).

Protein-membrane association assay

E. coli BL21(DE3) carrying wild-type or mutated (M1, M2, and M3) Rt-PmtA was cultured in Luria-Bertani medium containing ampicillin (100 mg/ml) at 37°C with vigorous shaking at 160 rpm until OD_{600} reached 0.4 to 0.5. The induction was initiated by 0.5 mM IPTG and subsequently maintained at 37°C and 160 rpm for 3 hours. The cells were lysed with low phosphate buffer [3 mM Na_2HPO_4 and 1.1 mM KH_2PO_4 (pH 7.3)] up to 60-ml volume. Cells were disrupted following the method above. The lysate was divided into 10-ml aliquots. An additional 700 mM NaCl in low phosphate buffer (pH 7.3) was added to make 150, 250, 350, and 500 mM NaCl and incubated in room temperature for 20 min on 3D rocker. The incubated lysed cells were centrifuged to remove cell debris (21,672 rcf at 4°C) for 1.5 hours, and 25 ml of each supernatant was transferred for further separation between membrane and soluble fractions via high-speed centrifugation for 1 hour at 4°C (120,000 rcf; Beckmann Optima TL ultracentrifuge with rotor Ti70) (*54*). The soluble fraction was isolated, whereas the membrane pellet was further resuspended with low phosphate buffer containing 0.1% SDS. The equal amount of each fraction was analyzed through 12% SDS–polyacrylamide gel electrophoresis and Western blot using the 6×His-tag antibody horseradish peroxidase conjugate (Abcam, UK).

Rt-PmtA's biological assembly analysis

The wild-type Rt-PmtA was expressed and purified in similar condition as in "protein expression and purification" step. The method was slightly modified by conducting the purification under DDM scarce condition. The DDM was not included in all buffers used in purification, except the solubilization step. The purified Rt-PmtA was eluted from SEC column (Superdex 75 10/300 GL, GE Healthcare) in final buffer B.

CD spectroscopy of Rt-PmtA wild-type and mutants

CD spectroscopy was conducted to confirm the structural integrity of wild-type and mutants. The purified wild-type and mutants were

prepared at concentration of 0.1 mg/ml (equal to 4 μM) in 10 mM sodium phosphate (pH 7.5), with 300-μl total volume. The CD spectra of wild type and mutants were recorded 10 times between 190 and 260 nm by Jasco J-815 CD spectrometer at 20°C. The final spectra were obtained from the average measurements of 10 scans and normalized against buffer.

Supplementary Materials

This PDF file includes:

Figs. S1 to S9
Optimized Gene of Rt-PmtA
Table S1

REFERENCES AND NOTES

1. R. Ernst, C. S. Ejsing, B. Antonny, Homeoviscous adaptation and the regulation of membrane lipids. *J. Mol. Biol.* **428**, 4776–4791 (2016).
2. S. Furse, A. I. P. M. de Kroon, Phosphatidylcholine's functions beyond that of a membrane brick. *Mol. Membr. Biol.* **32**, 117–119 (2015).
3. T. Hanada, Y. Kashima, A. Kosugi, Y. Koizumi, F. Yanagida, S. Udaka, A gene encoding phosphatidylethanolamine N-methyltransferase from Acetobacter aceti and some properties of its disruptant. *Biosci. Biotechnol. Biochem.* **65**, 2741–2748 (2001).
4. K. E. E. de Rudder, I. M. Löpez-Lara, O. Geiger, Inactivation of the gene for phospholipid *N*-methyltransferase in *Sinorhizobium meliloti*: Phosphatidylcholine is required for normal growth. *Mol. Microbiol.* **37**, 763–772 (2000).
5. X. Liu, Y. Sun, F. Cao, M. Xiong, S. Yang, Y. Li, X. Yu, Y. Li, X. Wang, Absence of phosphatidylcholine in bacterial membranes facilitates translocation of Sec-dependent β-lactamase AmpC from cytoplasm to periplasm in two *Pseudomonas* strains. *Microb. Pathog.* **106**, 94–102 (2017).
6. P. J. Wilderman, A. I. Vasil, W. E. Martin, R. C. Murphy, M. L. Vasil, *Pseudomonas aeruginosa* synthesizes phosphatidylcholine by use of the phosphatidylcholine synthase pathway. *J. Bacteriol.* **184**, 4792–4799 (2002).
7. M. Wessel, S. Klüsener, J. Gödeke, C. Fritz, S. Hacker, F. Narberhaus, Virulence of *Agrobacterium tumefaciens* requires phosphatidylcholine in the bacterial membrane. *Mol. Microbiol.* **62**, 906–915 (2006).
8. M. Bogdanov, M. Umeda, W. Dowhan, Phospholipid-assisted refolding of an integral membrane protein: Minimum structural features for phosphatidylethanolamine to act as a molecular chaperone. *J. Biol. Chem.* **274**, 12339–12345 (1999).
9. G. van Meer, D. R. Voelker, G. W. Feigenson, Membrane lipids: Where they are and how they behave. *Nat. Rev. Mol. Cell Biol.* **9**, 112–124 (2008).
10. O. Geiger, I. M. López-Lara, C. Sohlenkamp, Phosphatidylcholine biosynthesis and function in bacteria. *Biochim. Biophys. Acta* **1831**, 503–513 (2013).
11. D. B. Medeot, C. Sohlenkamp, M. S. Dardanelli, O. Geiger, M. García De Lema, I. M. López-Lara, Phosphatidylcholine levels of peanut-nodulating *Bradyrhizobium* sp. SEMIA 6144 affect cell size and motility. *FEMS Microbiol. Lett.* **303**, 123–131 (2010).
12. R. Conde-Alvarez, M. J. Grilló, S. P. Salcedo, M. J. de Miguel, E. Fugier, J. P. Gorvel, I. Moriyón, M. Iriarte, Synthesis of phosphatidylcholine, a typical eukaryotic phospholipid, is necessary for full virulence of the intracellular bacterial parasite *Brucella abortus*. *Cell. Microbiol.* **8**, 1322–1335 (2006).
13. L. R. Joyce, Z. Guan, K. L. Palmer, Phosphatidylcholine biosynthesis in mitis group streptococci via host metabolite scavenging. *J. Bacteriol.* **201**, e00495-19 (2019).
14. G. M. Conover, F. Martinez-Morales, M. I. Heidtman, Z.-Q. Luo, M. Tang, C. Chen, O. Geiger, R. R. Isberg, Phosphatidylcholine synthesis is required for optimal function of *Legionella pneumophila* virulence determinants. *Cell. Microbiol.* **10**, 514–528 (2008).
15. M. Aktas, S. Köster, S. Kizilirmak, J. C. Casanova, H. Betz, C. Fritz, R. Moser, Ö. Yildiz, F. Narberhaus, Enzymatic properties and substrate specificity of a bacterial phosphatidylcholine synthase. *FEBS J.* **281**, 3523–3541 (2014).
16. C. Sohlenkamp, I. M. López-Lara, O. Geiger, Biosynthesis of phosphatidylcholine in bacteria. *Prog. Lipid Res.* **42**, 115–162 (2003).
17. B. V. R. Sastry, C. N. Statham, J. Axelrod, F. Hirata, Evidence for two methyltransferases involved in the conversion of phosphatidylethanolamine to phosphatidylcholine in the rat liver. *Arch. Biochem. Biophys.* **211**, 762–773 (1981).
18. M. I. Kanipes, S. A. Henry, The phospholipid methyltransferases in yeast. *Biochim. Biophys. Acta* **1348**, 134–141 (1997).
19. T. Kodaki, S. Yamashita, Yeast phosphatidylethanolamine methylation pathway. Cloning and characterization of two distinct methyltransferase genes. *J. Biol. Chem.* **262**, 15428–15435 (1987).
20. M. Aktas, F. Narberhaus, In vitro characterization of the enzyme properties of the phospholipid *N*-methyltransferase PmtA from *Agrobacterium tumefaciens*. *J. Bacteriol.* **191**, 2033–2041 (2009).
21. L. Danne, M. Aktas, J. Gleichenhagen, N. Grund, D. Wagner, H. Schwalbe, B. Hoffknecht, N. Metzler-Nolte, F. Narberhaus, Membrane-binding mechanism of a bacterial phospholipid N-methyltransferase. *Mol. Microbiol.* **95**, 313–331 (2015).
22. L. Danne, M. Aktas, N. Grund, T. Bentler, R. Erdmann, F. Narberhaus, Dissection of membrane-binding and -remodeling regions in two classes of bacterial phospholipid *N*-methyltransferases. *Biochim. Biophys. Acta Biomembr.* **1859**, 2279–2288 (2017).
23. D. J. Shields, R. Lehner, L. B. Agellon, D. E. Vance, Membrane topography of human phosphatidylethanolamine *N*-methyltransferase. *J. Biol. Chem.* **278**, 2956–2962 (2003).
24. M. Aktas, M. Wessel, S. Hacker, S. Klüsener, J. Gleichenhagen, F. Narberhaus, Phosphatidylcholine biosynthesis and its significance in bacteria interacting with eukaryotic cells. *Eur. J. Cell Biol.* **89**, 888–894 (2010).
25. J. Kleetz, L. Welter, A.-S. Mizza, M. Aktas, F. Narberhaus, Phospholipid *N*-methyltransferases produce various methylated phosphatidylethanolamine derivatives in thermophilic bacteria. *Appl. Environ. Microbiol.* **87**, e0110521 (2021).
26. E. B. M. Denner, M. Kolari, D. Hoornstra, I. Tsitko, P. Kämpfer, H.-J. Busse, M. Salkinoja-Salonen, *Rubellimicrobium thermophilum* gen. nov., sp. nov., a red-pigmented, moderately thermophilic bacterium isolated from coloured slime deposits in paper machines. *Int. J. Syst. Evol. Microbiol.* **56**, 1355–1362 (2006).
27. L. Li, S. Nachtergaele, A. M. Seddon, V. Tereshko, N. Ponomarenko, R. F. Ismagilov, Simple host-guest chemistry to modulate the process of concentration and crystallization of membrane proteins by detergent capture in a microfluidic device. *J. Am. Chem. Soc.* **130**, 14324–14328 (2008).
28. Z. Li, Y. Tang, Y. Wu, S. Zhao, J. Bao, Y. Luo, D. Li, Structural insights into the committed step of bacterial phospholipid biosynthesis. *Nat. Commun.* **8**, 1691 (2017).
29. G. A. Signorell, T. C. Kaufmann, W. Kukulski, A. Engel, H. W. Rémigy, Controlled 2D crystallization of membrane proteins using methyl-β-cyclodextrin. *J. Struct. Biol.* **157**, 321–328 (2007).
30. J. L. Martin, F. M. McMillan, SAM (dependent) I AM: The S-adenosylmethionine-dependent methyltransferase fold. *Curr. Opin. Struct. Biol.* **12**, 783–793 (2002).
31. A. Jurcik, D. Bednar, J. Byska, S. M. Marques, K. Furmanova, L. Daniel, P. Kokkonen, J. Brezovsky, O. Strnad, J. Stourac, A. Pavelka, M. Manak, J. Damborsky, B. Kozlikova, CAVER Analyst 2.0: Analysis and visualization of channels and tunnels in protein structures and molecular dynamics trajectories. *Bioinformatics* **34**, 3586–3588 (2018).
32. M. Aktas, J. Gleichenhagen, R. Stoll, F. Narberhaus, *S*-adenosylmethionine-binding properties of a bacterial phospholipid *N*-methyltransferase. *J. Bacteriol.* **193**, 3473–3481 (2011).
33. A. L. Lomize, S. C. Todd, I. D. Pogozheva, Spatial arrangement of proteins in planar and curved membranes by PPM 3.0. *Protein Sci.* **31**, 209–220 (2022).
34. L. Holm, A. Laiho, P. Törönen, M. Salgado, DALI shines a light on remote homologs: One hundred discoveries. *Protein Sci.* **32**, e4519 (2023).
35. M. Varadi, S. Anyango, M. Deshpande, S. Nair, C. Natassia, G. Yordanova, D. Yuan, O. Stroe, G. Wood, A. Laydon, A. Zídek, T. Green, K. Tunyasuvunakool, S. Petersen, J. Jumper, E. Clancy, R. Green, A. Vora, M. Lutfi, M. Figurnov, A. Cowie, N. Hobbs, P. Kohli, G. Kleywegt, E. Birney, D. Hassabis, S. Velankar, AlphaFold protein structure database: Massively expanding the structural coverage of protein-sequence space with high-accuracy models. *Nucleic Acids Res.* **50**, D439–D444 (2022).
36. L. Danne, M. Aktas, A. Unger, W. A. Linke, R. Erdmann, F. Narberhaus, Membrane remodeling by a bacterial phospholipid-methylating enzyme. *mBio* **8**, e02082-16 (2017).
37. B. K. Bhandari, C. S. Lim, P. P. Gardner, TISIGNER.com: Web services for improving recombinant protein production. *Nucleic Acids Res.* **49**, W654–W661 (2021).
38. J. García-Nafría, J. F. Watson, I. H. Greger, IVA cloning: A single-tube universal cloning system exploiting bacterial In vivo assembly. *Sci. Rep.* **6**, 27459 (2016).
39. G. D. van Duyne, R. F. Standaert, P. A. Karplus, S. L. Schreiber, J. Clardy, Atomic structures of the human immunophilin FKBP-12 complexes with FK506 and rapamycin. *J. Mol. Biol.* **229**, 105–124 (1993).
40. D. Li, M. Caffrey, Renaturing membrane proteins in the lipid cubic hhase, a nanoporous membrane mimetic. *Sci. Rep.* **4**, 5806 (2014).
41. A. Urbani, T. Warne, A colorimetric determination for glycosidic and bile salt-based detergents: Applications in membrane protein research. *Anal. Biochem.* **336**, 117–124 (2005).
42. J. Folch, M. Lees, G. H. S. Stanley, A simple method for the isolation and purification of total lipides from animal tissues. *J. Biol. Chem.* **226**, 497–509 (1957).
43. D. S. Wishart, A. C. Guo, E. Oler, F. Wang, A. Anjum, H. Peters, R. Dizon, Z. Sayeeda, S. Tian, B. L. Lee, M. Berjanskii, R. Mah, M. Yamamoto, J. Jovel, C. Torres-Calzada, M. Hiebert-Giesbrecht, V. W. Lui, D. Varshavi, D. Varshavi, D. Allen, D. Arndt, N. Khetarpal, A. Sivakumaran, K. Harford, S. Sanford, K. Yee, X. Cao, Z. Budinski, J. Liigand, L. Zhang,

J. Zheng, R. Mandal, N. Karu, M. Dambrova, H. B. Schiöth, R. Greiner, V. Gautam, HMDB 5.0: The human metabolome database for 2022. *Nucleic Acids Res.* **50**, D622–D631 (2022).
44. M. Sud, E. Fahy, D. Cotter, A. Brown, E. A. Dennis, C. K. Glass, A. H. Merrill, R. C. Murphy, C. R. H. Raetz, D. W. Russell, S. Subramaniam, LMSD: LIPID MAPS structure database. *Nucleic Acids Res.* **35**, D527–D532 (2007).
45. T. Pluskal, S. Castillo, A. Villar-Briones, M. Orešič, MZmine 2: Modular framework for processing, visualizing, and analyzing mass spectrometry-based molecular profile data. *BMC Bioinformatics* **11**, 395 (2010).
46. J. Yoo, J. Lee, J. Kim, Structural basis for the selective methylation of 5-carboxymethoxyuridine in tRNA modification. *Nucleic Acids Res.* **51**, 9432–9441 (2023).
47. C. Vonrhein, C. Flensburg, P. Keller, A. Sharff, O. Smart, W. Paciorek, T. Womack, G. Bricogne, Data processing and analysis with the *autoPROC* toolbox. *Acta Crystallogr. D Biol. Crystallogr.* **67**, 293–302 (2011).
48. P. Skubak, D. Arac, M. W. Bowler, A. R. Correia, A. Hoelz, S. Larsen, G. A. Leonard, A. A. McCarthy, S. McSweeney, C. Mueller-Dieckmann, H. Otten, G. Salzman, N. S. Pannua, A new MR-SAD algorithm for the automatic building of protein models from low-resolution x-ray data and a poor starting model. *IUCrJ* **5**, 166–171 (2018).
49. P. Skubák, N. S. Pannu, Automatic protein structure solution from weak x-ray data. *Nat. Commun.* **4**, 2777 (2013).
50. E. Krissinel, A. A. Lebedev, V. Uski, C. B. Ballard, R. M. Keegan, O. Kovalevskiy, R. A. Nicholls, N. S. Pannu, P. Skubák, J. Berrisford, M. Fando, B. Lohkamp, M. Wojdyr, A. J. Simpkin, J. M. H. Thomas, C. Oliver, C. Vonrhein, G. Chojnowski, A. Basle, A. Purkiss, M. N. Isupov, S. Mcnicholas, E. Lowe, J. Trivinõ, K. Cowtan, J. Agirre, D. J. Rigden, I. Uson, V. Lamzin, I. Tews, G. Bricogne, A. G. W. Leslie, D. G. Brown, S. Antonyuk, CCP4 Cloud for structure determination and project management in macromolecular crystallography. *Acta Crystallogr. D Struct. Biol.* **78**, 1079–1089 (2022).
51. P. Emsley, B. Lohkamp, W. G. Scott, K. Cowtan, Features and development of Coot. *Acta Crystallogr. D Biol. Crystallogr.* **66**, 486–501 (2010).
52. G. N. Murshudov, P. Skubák, A. A. Lebedev, N. S. Pannu, R. A. Steiner, R. A. Nicholls, M. D. Winn, F. Long, A. A. Vagin, *REFMAC5* for the refinement of macromolecular crystal structures. *Acta Crystallogr. D Struct. Biol.* **67**, 355–367 (2011).
53. L. L. C. Schrödinger, The PyMOL molecular graphics system, Version ~1.8 (2015).
54. G. Cho, E. Lee, J. Kim, Structural insights into phosphatidylethanolamine formation in bacterial membrane biogenesis. *Sci. Rep.* **11**, 5785 (2021).

Acknowledgments: We thank beamline 5C of Pohang Accelerator Laboratory (South Korea) for providing access to synchrotron radiation facilities and technical support on x-ray Rt-PmtA data collection. We also acknowledge the GIST Advanced Institute of Instrumental Analysis (GAIA) for support and service in MS. **Funding:** This work was supported by National Research Foundation of Korea (RS-2024-00411137) and GIST Research Institute (GRI) grant funded by the GIST. **Author contributions:** Conceptualization, writing—original draft, and writing—review and editing: S.D.S. and J.K. Methodology, resources, funding acquisition, data curation, validation, supervision, and project administration: J.K. Investigation and visualization: S.D.S. **Competing interests:** The authors declare that they have no competing interests. **Data and materials availability:** The atomic coordinates and structure factors for Rt-PmtA complexed with $DMPE^{18:1/18:1}$, SAH, and DDM are deposited to Protein Data Bank (PDB) under accession code 8YS9. All data needed to evaluate the conclusions in the paper are present in the paper and/or the Supplementary Materials.

Submitted 11 June 2024
Accepted 26 August 2024
Published 2 October 2024
10.1126/sciadv.adr0122